Chinese Journal of Chemical Engineering 67 (2024) 220–227

Contents lists available at ScienceDirect

Chinese Journal of Chemical Engineering

journal homepage: www.elsevier.com/locate/CJChE

Full Length Article

Production of linear alkylbenzene over Ce containing Beta zeolites

Shiqi Zhang [1, 2], Shengzhi Gan [1, 2], Baoyu Liu [1, 2, *], Jinxiang Dong [1, 2]

[1] School of Chemical Engineering and Light Industry, Guangdong Provincial Key Laboratory of Plant Resources Biorefinery, Guangzhou Key Laboratory of Clean Transportation Energy Chemistry, Guangdong University of Technology, Guangzhou 510006, China
[2] Jieyang Branch of Chemistry and Chemical Engineering Guangdong Laboratory (Rongjiang Laboratory), Jieyang 515200, China

ARTICLE INFO

Article history:
Received 22 June 2023
Received in revised form
15 November 2023
Accepted 15 November 2023
Available online 30 November 2023

Keywords:
Beta zeolites
Catalysis
Alkylation
Long-chain olefins

ABSTRACT

Ce-encapsulated Beta zeolite was synthesized by a one-pot hydrothermal method with citric acid complexing Ce in the absence of Na species. Additional citric acid can effectively prevent the deposition of Ce species during the hydrothermal synthesis of zeolites, leading to uniform distribution of Ce cluster in the framework of Beta zeolites. Moreover, the sodium-free synthesis system resulted that the Brønsted acid sites were mainly located on the straight channels and external surface of Beta zeolites, improving the utilization of Brønsted acid sites. In addition, Ce encapsulated Beta zeolites showed enhanced activity and robust stability in the alkylation of benzene with 1-dodecene based on the synergistic effect between Ce species and Brønsted acid sites, which pave the way for its practical application in the production of alkylbenzene.

1. Introduction

Alkylbenzene is a significant chemical intermediate, and its sulfonated product–alkylbenzene sulfonate plays a vital role as an anionic surfactant that can be widely used in field of detergents [1,2]. Considering serious environmental issues related to the extensive use of synthetic detergents, the environmental safety of detergents has attracted widespread attention [3]. In the early 1960s, it is found that linear alkylbenzene sulfonates (LAS) have stronger degradation ability with low pollution toward environment than branched alkylbenzene sulfonates (BAS), and branched alkylbenzene (BAB) has been gradually replaced by linear alkylbenzene (LAB) [4].

In industrial production, benzene reacts with long-chain α-olefins or chlorinated alkanes (C_{10}–C_{14}) to produce LAB by using acid catalysts. The LAB has different isomers, such as 2-, 3-, 4-, 5-, 6-LABs, among which 2-LAB exhibits the highest biodegradability and detergency [5–7]. Homogeneous catalysts, such as $AlCl_3$ and HF, are mainly used in industrial production, but their selectivity toward 2-LAB is low, *i.e.*, the selectivity of $AlCl_3$ is only about 30%, and that of HF is only 15%–18% [8–10]. At the same time, these homogeneous catalysts also have some drawbacks such as corrosion of equipment, environmental pollution, and separation difficulty [11]. Consequently, it is highly desired to develop an environmental friendly catalysis technology with a high selectivity of 2-LAB in the production of LAB. In the past decades, the tremendous efforts have been made to develop green technology for production of LAB, such as ionic liquids [12–14], heteropoly acids [15–17], ion exchange resins [18], sulfated zirconia [19], clays [20], and zeolites [21–24]. Among them, zeolites have attracted high attention due to their unique pore structure, tunable acidity, and high 2-LAB selectivity.

Currently, the mordenite (MOR) [25], Beta [5,26], and faujasite (FAU) [22,27] zeolites with large pore have been intensively investigated. Among these, the Beta zeolite is a promising solid acid catalyst in the production of LAB because it has large twelve-member ring channels with a pore size of 0.55 nm × 0.55 nm in zigzag channels and 0.64 nm × 0.76 nm in straight channels [28]. The size of the straight channel pore is similar to the size of 2-LAB (0.53 nm × 0.72 nm) [3], which is benefit for the formation of 2-LAB based on the shape selectivity. However, the short lifetime impends its application in the production of LAB [9]. The modification of zeolites by loading rare earth metal is an effective strategy to improve the stability of zeolites in the alkylation of aromatics [29,30]. However, the metal precursors usually form the precipitate as colloidal oxyhydroxides under the required pH and temperatures for zeolite synthesis [31,32], which makes that the fabrication of rare earth metal encapsulated zeolites is rather difficult [33].

* Corresponding author at: Faculty of Chemical Engineering and Light Industry, Guangdong University of Technology, Guangzhou 510006, China.
E-mail address: baoyu.liu@gdut.edu.cn (B. Liu).

https://doi.org/10.1016/j.cjche.2023.11.007
1004-9541/

In this study, Ce-encapsulated Beta zeolites are fabricated by a one-pot hydrothermal method by using citric acid as a ligand in the absence of Na species. The additional citric acid can stabilize the Ce cations and guide the formation of self-assembly structure between zeolitic building units and citric acid-stabilized precursors through the electrostatic and dispersion interactions, which can strongly inhibit the formation of precipitation for Ce cationic moieties as colloidal oxyhydroxides during hydrothermal synthesis of Beta zeolites, resulting in the generation of Ce encapsulated Beta zeolites. The sodium-free synthesis system not only avoids the complicated ion-exchange process for transformation of type Na^+ to type H^+ but also confirms that the most Brønsted acid sites are located on the external surface and in the straight channels of Beta zeolite, improving the alkylation efficiency. The obtained Ce encapsulated Beta-zeolite exhibits superior catalytic activity and robust stability in the alkylation between benzene with 1-dodecene.

2. Experimental

2.1. Synthesis of catalysts

In the absence of sodium, Ce encapsulated Beta zeolites were prepared by a one-pot hydrothermal method by using citric acid as an organic ligand to stabilize Ce species, and the synthesis details can be found in experimental procedures section of the Supplementary Material.

2.2. Catalytic tests

The catalytic performance of obtained Beta zeolite was evaluated by the liquid-phase alkylation between benzene with the 1-dodecene. Before the catalytic test, the samples were granulated (0.42–0.85 nm) and activated at 400 °C for 2 h. The liquid-phase alkylation between benzene and 1-dodecene was carried out in a fixed bed microreactor. The reaction condition was atmospheric pressure, 80 °C, and the weight hourly space velocity (WHSV) was 40 h^{-1}. The molar ratio of benzene to 1-dodecene was 8.75, and ethyl cyclohexane was the internal standard substance. The reaction liquid was periodically collected and analyzed by using the Agilent 7820A gas chromatograph equipped with HP-5 chromatographic column and flame ionization detector for detection. The 1-dodecene conversion (C) and 2-LAB selectivity (S) were calculated as follows:

$$C = \frac{C_{A_0} - C_A}{C_{A_0}} \times 100\% \quad (1)$$

$$S = \frac{n_{2\text{-LAB}}}{\sum_{i=2}^{6} n_{i\text{-LAB}}} \times 100\% \quad (2)$$

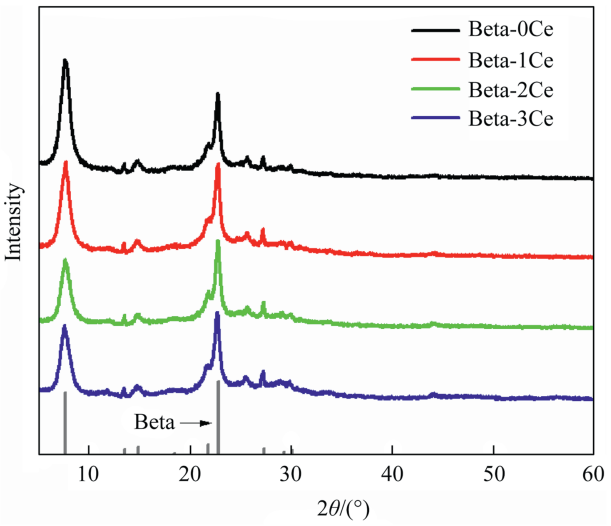

Fig. 1. XRD patterns of resultant Beta zeolites.

where C_{A_0} is the concentration of 1-dodecene in raw material (mmol·L^{-1}), C_A is the concentration of 1-dodecene in the reaction solution (mmol·L^{-1}), and n_{i-LAB} (i = 2,3,4,5,6) is the molar amount of i-LAB isomer (mmol).

3. Results and Discussion

3.1. Characterization of Ce encapsulated Beta zeolite

The X-ray diffraction (XRD) patterns of the synthesized Ce-encapsulated Beta zeolites are shown in Fig. 1. All samples exhibit typical diffraction peaks of Beta zeolite at about 7.6° and 22.5° 2θ (the gray column at the bottom of Fig. 1 represents the standard XRD pattern of Beta zeolite), and no other impurities are observed, indicating that pure and well-crystallized Beta zeolites are obtained in present research. However, the diffraction peak intensity of Ce-loaded Beta zeolites is lower than that of Beta-0Ce sample, suggesting that the introduction of Ce species reduces the crystallinity of zeolite on a certain degree. At the same time, no Ce oxide diffraction peaks are found, which is related to the high dispersion of Ce species in the zeolitic framework owing to the absence of large metal clusters. The elemental content of the prepared samples is characterized by inductively coupled plasma optical emission spectrometer (ICP-OES) (Table 1), it is found from Table 1 that the Si/Al ratio of these samples is almost the same with or without Ce species, indicating that the additional Ce species do not affect the Si/Al ratio of the sample.

The chemical state of Ce species in typical Beta-3Ce is characterized by X-ray photoelectron spectroscopy (XPS), and the results are shown in Fig. 2. The peaks at ~917 and ~886 eV are

Table 1
Textural properties and elemental analysis of Beta zeolites

Catalyst	S_{Beta}①/$m^2 \cdot g^{-1}$	S_{ext}②/$m^2 \cdot g^{-1}$	S_{mic}②/$m^2 \cdot g^{-1}$	V_{tol}③/$cm^3 \cdot g^{-1}$	V_{mic}③/$cm^3 \cdot g^{-1}$	V_{meso}④/$cm^3 \cdot g^{-1}$	Elements content/% (mass)			Si/Al
							Si	Al	Ce	
Beta-0Ce	618	93	525	0.660	0.203	0.457	47.107	1.001	–	45
Beta-1Ce	648	87	561	0.578	0.216	0.362	43.068	0.954	0.283	43
Beta-2Ce	605	82	523	0.456	0.202	0.254	44.246	1.040	0.933	41
Beta-3Ce	563	92	471	0.331	0.183	0.148	41.708	0.922	2.469	43

① Total surface area was obtained by the BET method.
② Determined from the t-plot method.
③ Determined from the adsorbed volume at P/P_0 = 0.99.
④ $V_{mes} = V_{tol} - V_{mic}$.

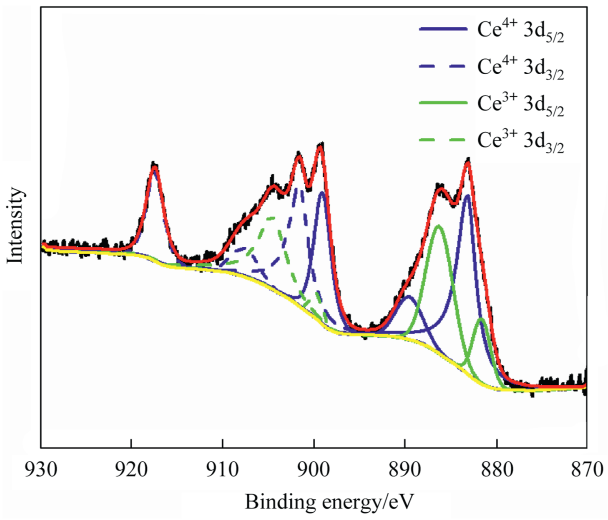

Fig. 2. Ce $3d_{3/2,5/2}$ XPS spectra collected for Beta-3Ce.

characteristic for Ce^{4+} and Ce^{3+} species, respectively. These data are further analyzed by using Avantage software and compared with literature data [34,35], as shown in Table S1, Supplementary Material. The Ce 3d binding energy of Beta-3Ce is divided into 10 peaks, and the relative content of Ce species with different valences is calculated according to the corresponding total peak area. It is observed from Table S1 that Ce species mainly exist in the form of Ce^{4+}, and the fraction of Ce^{4+} species in the Beta-3Ce zeolite is almost 65%.

The morphology of the prepared Beta zeolites is characterized using scanning electron microscopy (SEM), as shown in Fig. 3. All samples exhibit the morphology of ellipsoidal particles, the corresponding mean particle sizes of Beta-0Ce, Beta-1Ce, Beta-2Ce, and Beta-3Ce are 126, 162, 191, and 264 nm, respectively (Fig. S1), which gradually increase with increasing the amount of Ce species. At the same time, the dispersion of Ce cluster in the Beta zeolitic framework is characterized by high angle angular dark field-scanning transmission electron microscopy (HAADF-STEM), as shown in Fig. 4, and the particle size distributions and dispersity index (DI) [36] of Ce clusters for various Ce encapsulated Beta zeolites are given in Figs. 5 and 6, respectively. It is found from Figs. 5 and 6 that Ce clusters size is very uniform in resultant zeolites and Ce clusters size increases from 2.37 nm for Beta-1Ce to 3.06 nm for Beta-3Ce with increasing Ce loading.

The N_2 adsorption–desorption isotherms and textural parameters of obtained samples are shown in Fig. 7 and Table 1, respectively. It is observed from Fig. 7 that all samples exhibit characteristics of micropore materials, and the additional sharp increase in nitrogen uptakes in a relatively pressure of $P/P_0 > 0.9$ is reasonably attributed to the voids of stacked zeolite particles. In addition, the total volume (V_{tol}) and micropore volume (V_{mic}) of Beta-*x*Ce samples decreased in the order of Beta-0Ce>Beta-1Ce>Beta-2Ce>Beta-3Ce (Table 1), indicating that additional large Ce clusters can block the pore channels of Beta zeolites, leading to inferior diffusion properties of Beta zeolites for guest molecules on a certain degree.

It is known to everyone that the concentration of Bronsted acid sites in zeolite is strongly related to their catalytic performance in the alkylation reaction. In present research, the acidity of zeolites is characterized by employing various organic basic molecular as the probes. The kinetic diameter of pyridine is small (~0.54 nm) [37], which can enter all channels of Beta zeolites and be used to detect the total Bronsted acid concentration of the obtained sample. Due to the large size of benzene (kinetic diameter is ~0.62 nm) [38], it can only react with dodecyl carbenium ions in the twelve-member ring straight channel and the external surface of the Beta zeolites. Here, the 2,4,6-trimethylpyridine is large (~0.62 nm) that cannot enter the zigzag channel of the zeolite [39]. Thus, it is used to detect the concentration of Bronsted acid sites in the straight channel and the external surface of Beta zeolites. Moreover, the 2,6-di-*tert*-butylpyridine with a kinetic diameter of ~0.79 nm [37] cannot enter the interior of Beta zeolite, so it is used as a probe molecule to detect the concentration of Bronsted acid sites located on the external surface of Beta zeolites.

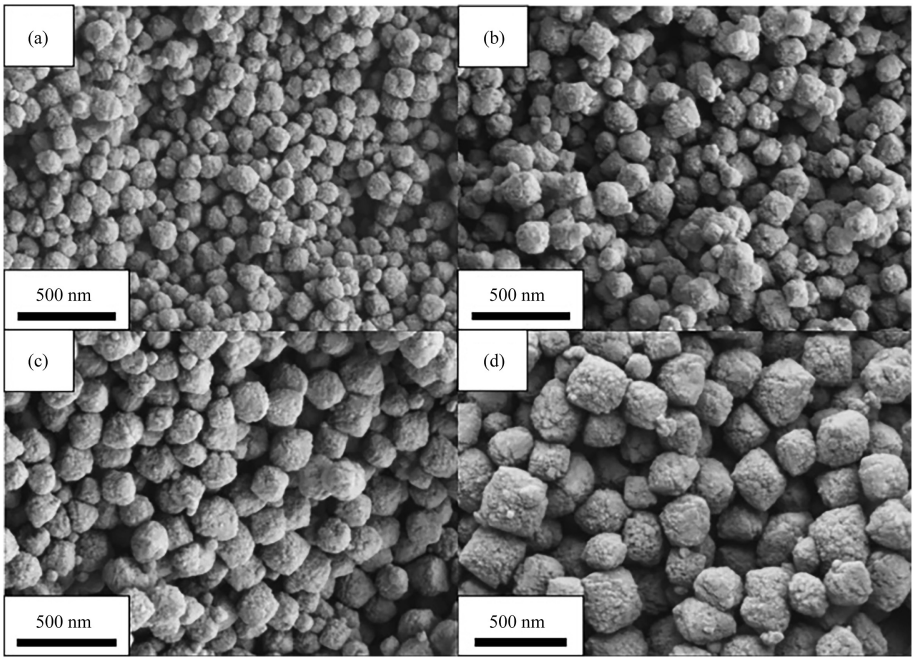

Fig. 3. SEM images of (a) Beta-0Ce, (b) Beta-1Ce, (c) Beta-2Ce, and (d) Beta-3Ce.

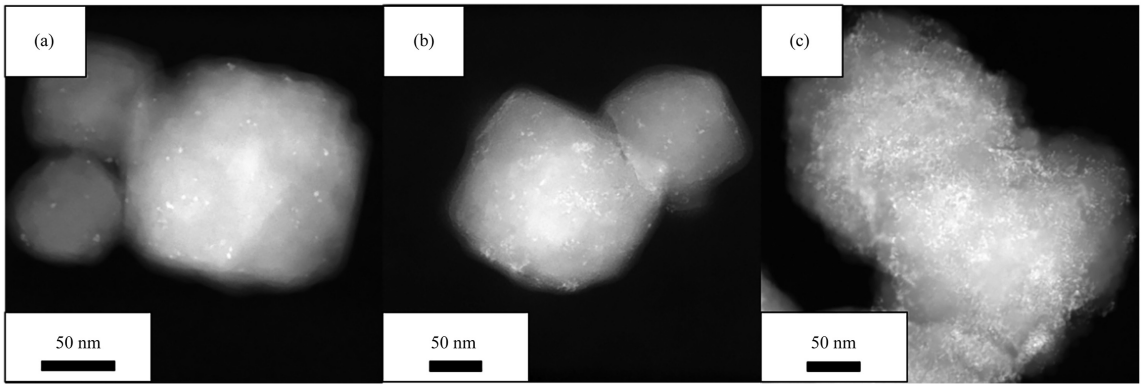

Fig. 4. HAADF-STEM images of (a) Beta-1Ce, (b) Beta-2Ce, and (c) Beta-3Ce, respectively.

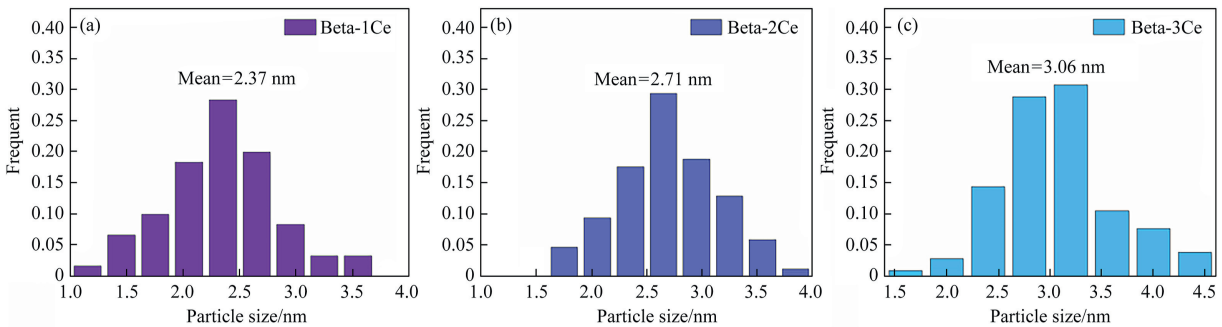

Fig. 5. Particle size distributions of Ce cluster in (a) Beta-1Ce, (b) Beta-2Ce, and (c) Beta-3Ce.

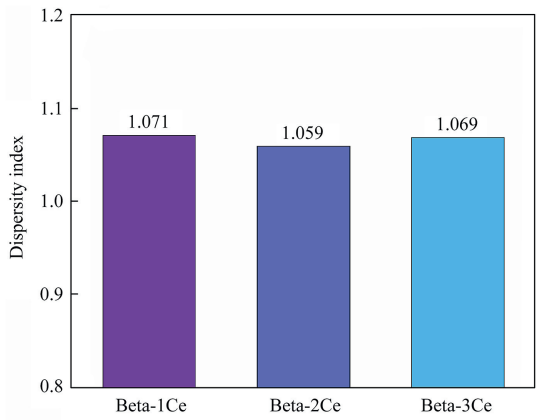

Fig. 6. Ce cluster dispersity index of resultant Beta zeolites from TEM characterization.

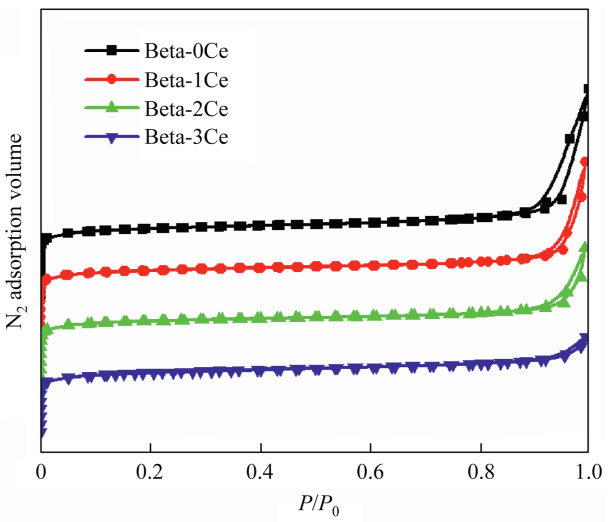

Fig. 7. N_2 adsorption–desorption isotherms of resultant Beta zeolites.

As shown in Fig. 8(a), the pyridine absorption peaks at ~1545 cm^{-1} and ~1455 cm^{-1} correspond to the Brønsted acid sites and Lewis acid sites, respectively [40,41]. The infrared spectrum of 2,4,6-trimethylpyridine adsorbed on the samples are shown in Fig. 8(b), the absorption peak at ~1638 cm^{-1} is originated from the Brønsted acid site [42] in the straight channel along *a* and *b* axis and on the external surface of Beta zeolites. Fig. 8(c) shows the infrared spectrum of 2,6-di-*tert*-butylpyridine adsorbed on the samples, it can be seen from Fig. 8(c) that all samples exhibit obvious absorption peaks at ~1616 cm^{-1}, corresponding to the Brønsted acid sites on the external surface of Beta zeolites [43,44]. Table S2 summarizes the acidity of obtained Beta zeolites, it is observed from Table S2 that most Brønsted acid sites of Beta zeolites located in the straight channels and the external surface, and the Bronsted acid sites are almost absent in the zigzag channels where the benzene cannot enter, which is attributed to the Na^+ free synthesis system in present work, and the proposed distribution of Brønsted acid sites in Beta zeolites is given in Fig. 9. The acidity of zeolites is from the coordinated Al species that are substituting for tetrahedral Si atom and are coordinated to generate the tricoordinated Al sites

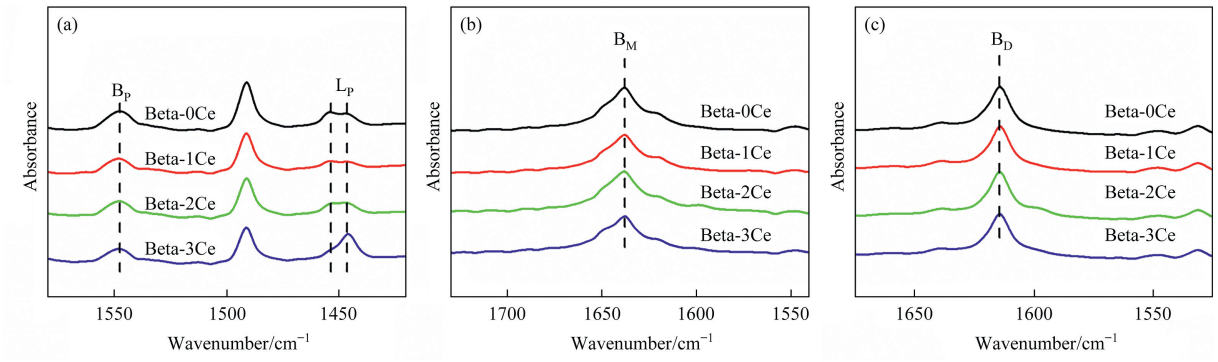

Fig. 8. FTIR spectra of pyridine (a), 2,4,6-trimethylpyridine (b), and 2,6-di-*tert*-butylpyridine (c) adsorption of resultant Beta zeolites.

and tetracoordinated Al sites. For tetracoordinated Al sites, the negative framework of zeolites can be compensated by the adsorption of H^+ ions, which forms the Si—OH^+—Al, becoming a Bronsted acid site. Therefore, the location of Al species is directly related to the distribution of Bronsted acid site of zeolites [45,46]. Here, the TEA^+ is employed as a structure-directing-agent to synthesize Beta zeolites without Na^+ species, and the TEA^+ has a large size (kinetic diameter is ~0.64 nm) [47], and it can only exist in the straight channels and external surface owing to the steric-hindrance effect. Thus, the Al species exclusively located in straight channels and the external surface based on the interaction between positive TEA^+ ions and negative $[AlO_4]^-$ species, which definitely influence the distribution of Bronsted acid sites of Beta zeolites, leading to observed results presented in Table S2.

At the same time, the ^1H MAS NMR (Magic Angle Spinning Nuclear Magnetic Resonance) spectra of typical Beta-0Ce and Beta-3Ce are given in Fig. S2, the peaks near 4×10^{-6} are assigned to Brønsted acid sites, and the peaks around 0.5×10^{-6}–2.5×10^{-6} are assigned to different silanol peaks [48–51]. It is observed from Fig. S2 that the concentration of Brønsted acid sites in Beta-0Ce is higher than in Beta-3Ce, which is consistent with the pyridine infrared data, but its chemical shift is smaller than that of Beta-3Ce. The higher chemical shift, the stronger acid strength of Brønsted acid sites [52], it indicates that the additional Ce species can improve the strength of Brønsted acid sites based on the Plank-Hirschler mechanism [53], which is beneficial to promoting the activity of Ce encapsulated Beta zeolites in the alkylation reaction.

3.2. Catalytic and regeneration performance of Ce encapsulated Beta zeolite

The catalytic performances of resultant Beta zeolites are evaluated in the liquid alkylation between benzene and 1-dodecene, as shown in Fig. S3 and Fig. 10. It is observed from Fig. S3 that the activity of typical Beta-3Ce gradually decreases with increasing the WHSV. Due to the limited time under laboratory conditions, the alkylation reaction is performed under harsh conditions with WHSV = 40 h^{-1} for Beta-*x*Ce samples, it is found that from Fig. 10 that the activity and lifetime of obtained Beta zeolites increase in the order of Beta-0Ce < Beta-1Ce < Beta-2Ce < Beta-3Ce, indicating that the additional Ce species can greatly enhance the activity of 1-dodece and suppress side reaction. At the same time, it can be found that Beta-3Ce—Na (the H^+ form Beta-3Ce is exchanged through Na^+ to shield all Bronsted acid sites of Beta-3Ce) has no catalytic activity, indicating that Ce active species only play an auxiliary role in the reaction rather than directly active the 1-dodece. According to previous research studies, Ce species have strong adsorption capacity for olefins [54–56].

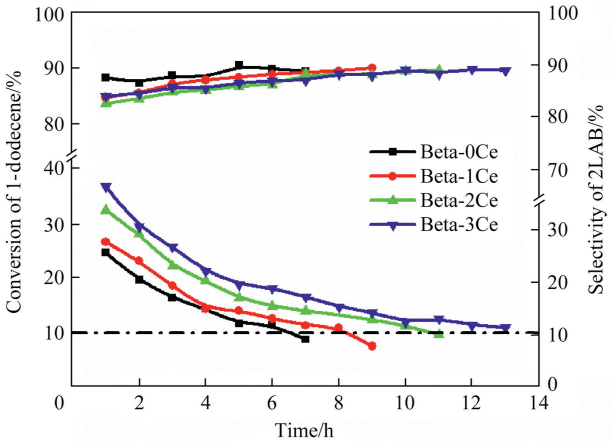

Fig. 10. Conversion of 1-Dodecene and Selectivity of 2-LAB of resultant Beta zeolites. LAB, linear alkylbenzene.

Moreover, the alkylation between benzene with 1-dodecene follows the Eley-Rideal mechanism, in which the adsorbed 1-dodecene on the acid sites is transformed into dodecyl carbenium ions that can react with free benzene in liquid phase rather than adsorbed benzene molecules, because the adsorbed benzene molecules on the acid sites decrease the electronic density on the aromatic ring that is very difficult for the electrophilic attack [57]. Therefore, it speculates that the additional Ce species can enhance the adsorption of 1-dodecene molecules through π-complexation [54–56], which improve the concentration of 1-dodecene near the Bronsted acid sites and definitely accelerate the production rate of dodecyl carbenium ions, resulting in high conversion of 1-

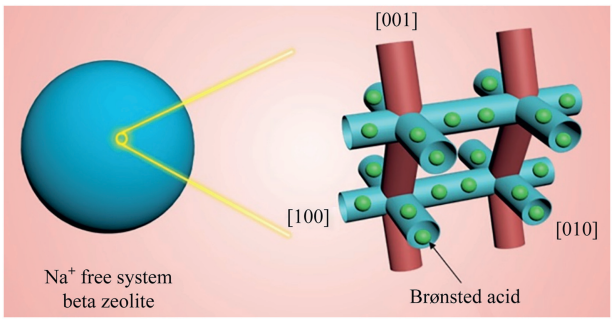

Fig. 9. Proposed distribution of Brønsted acid sites in Beta zeolites.

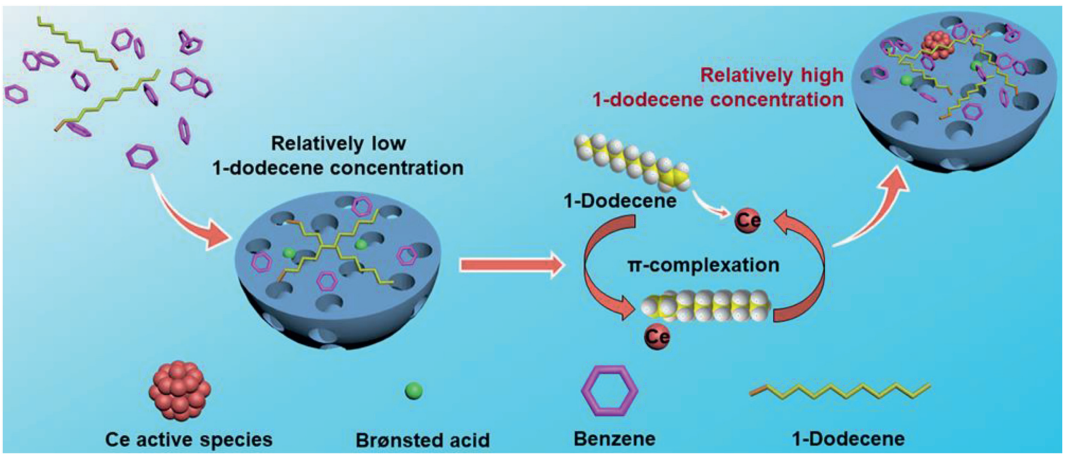

Fig. 11. Schematic diagram of the synergistic mechanism between Ce species and Bronsted acid sites for activating 1-dodecene.

dodecene, and the proposed synergistic mechanism between Ce species and Brønsted acid sites is shown in Fig. 11.

In addition, the Ce oxides can further active the benzene molecules in the form as presented in Fig. 12(a) [58], and the activated benzene is inclined to react with dodecyl carbenium ions. On the one hand, it can improve the alkylation efficiency between benzene and 1-dodecene, resulting in the formation of LAB products (Fig. 12(b)). On the other hand, it also inhibits the formation of oligomer arising from 1-dodecene through improving reaction activity between 1-dodecene with benzene, extending the lifetime of catalysts. Moreover, the thermogravimetric analysis (TGA) curves of spent Beta zeolites are given in Fig. S4, it is found that the resultant Beta zeolites exhibit discrepant coke content, and the corresponding coke generation rate for various Beta zeolites is presented in Table S3. It can be seen from Table S3 that the coke generation rate of Beta zeolites decreased in the order of Beta-0Ce > Beta-1Ce > Beta-2Ce > Beta-3Ce, indicating that additional Ce species can improve the stability of Beta zeolites in the alkylation, which is in agreement with above analysis.

Furthermore, the obtained Beta zeolites show a comparable selectivity towards 2-LAB (Fig. 10) due to the special shape-selectivity of Beta zeolitic topology. Especially, the Beta-3Ce, with the best catalytic property, is selected for the evaluation of stability. As shown in Fig. S5, the regenerative Ce encapsulated Beta zeolite (Beta-3Ce-R) exhibits similar selectivity of 2-LAB compared with fresh Beta-3Ce owing to the excellent shape-selectivity of Beta zeolites. However, the activity of Beta-3Ce-R shows a slighter decrease than Beta-3Ce, but the Beta-3Ce-R presents a comparable lifetime with Beta-3Ce, indicating that the resultant Beta-3Ce catalyst possesses robust stability.

In addition, the structure of Beta-3Ce, Beta-3Ce-R and spent Beta-3Ce after regeneration (Beta-3Ce-S) are further investigated by combination of XRD, SEM, FTIR spectra of pyridine and 2,6-di-*tert*-butylpyridine, N_2 adsorption–desorption isotherms and TGA technology. These results are shown in Figs. S6–S10, it is observed from Fig. S6 that the crystal structure of Beta zeolites is well maintained for all samples, but the intensity of the diffraction peaks for Beta-3Ce-S is lower than that of Beta-3Ce and Beta-3Ce-R, indicating that the crystallinity of Beta-3Ce-S is inferior compared with Beta-3Ce and Beta-3Ce-R. The SEM results (Fig. S7) show that Beta-3Ce-R still has ellipsoidal particles, but the grain size is slightly increased compared with Beta-3Ce due to Oswald ripening process during calcination. The acidity of Beta-3Ce and Beta-3Ce-R are shown in Fig. S8 and Table S4, it can be seen from Fig. S8 and Table S4 that both total Brønsted acid sites and external Brønsted acid sites of Beta-3Ce-R decrease compared with Beta-3Ce, indicating that regeneration process can lead to the loss of zeolitic acid sites owing to the calcination under high temperature.

The N_2 adsorption–desorption isotherm and textural properties of Beta-3Ce, Beta-3Ce-R and Beta-3Ce-S are given in Fig. S9 and Table S5, it is found that the micropore surface (S_{mic}) and micropore volume (V_{mic}) of Beta-3Ce-R is higher than those of Beta-3Ce, which is reasonably attributed to the fact that the particle size of

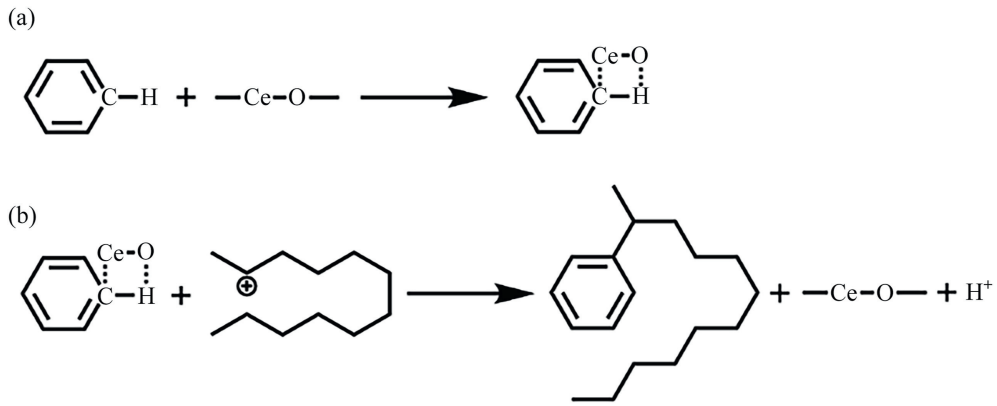

Fig. 12. Proposed reaction mechanism of alkylation of benzene with 1-dodecene on Ce-containing Beta zeolite: (a) activation of benzene on Ce species; (b) alkylation process between dodecyl carbenium ions with activated benzene.

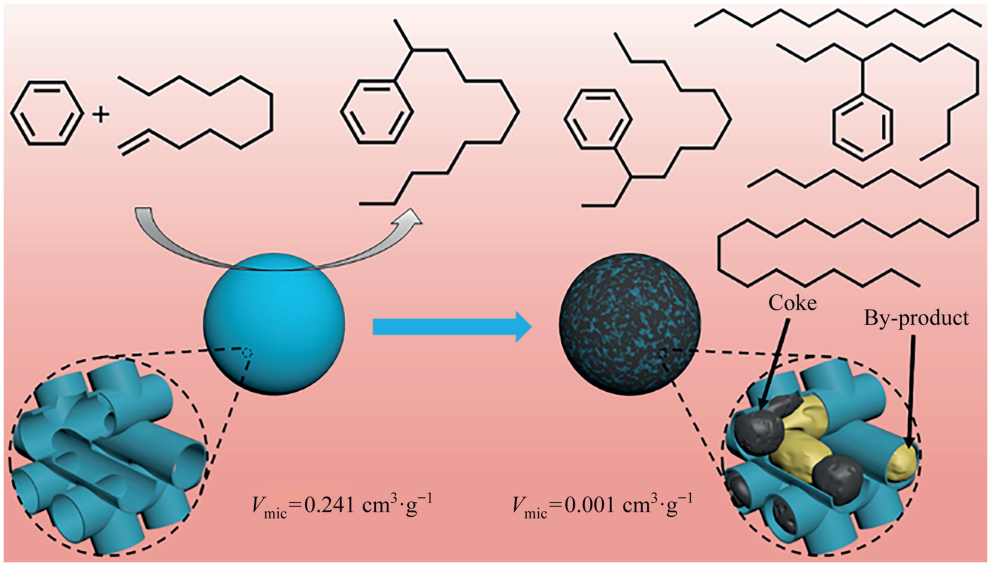

Fig. 13. Schematic diagram of carbon deposition in the channels of Beta-3Ce-R.

Beta-3Ce-R is larger than Beta-3Ce based on the SEM images (Fig. S7), it can improve the integrity of Beta zeolitic framework, leading to high value of S_{mic} and V_{mic} for Beta-3Ce-R. Moreover, the deactivated Beta-3Ce and Beta-3Ce-S showed the comparable content of hard coke (Fig. S10), it demonstrates that the resultant Beta-3Ce exhibits superior regeneration ability. Furthermore, the composition of soft cokes occluded in Beta-3Ce-S is analyzed by GC-MS, as shown in Fig. S11, it is observed that the compounds are very complex including isomers of LAB, various pyrolysis and oligomerization products of 1-dodecene, indicating that the alkylation between benzene with 1-dodecene undergoes a series of complex processes. The textural parameters of Beta-3Ce-S further verifies that the generated coke is mainly located in the interior of zeolitic framework, which completely blocks the channels of Beta zeolite, resulting in the deactivation of zeolite catalysts, and the proposed coke distribution is illustrated in Fig. 13.

4. Conclusions

The Ce containing Beta zeolites are successfully synthesized by employing citric acid as the ligand, which can effectively stabilize the Ce species in the synthesis gel of zeolites, resulting in the formation of Ce encapsulated Beta zeolites with uniform size of Ce clusters. In addition, the Brønsted acid sites of resultant Beta zeolites are mainly located in the straight channels and the external surface based on the Na free synthesis strategy, which improve the alkylation efficiency in the alkylation between benzene and 1-dodecene since the large size of benzene molecules are cannot enter into the zigzag channels of Beta zeolite owing to the steric hindrance effect. Moreover, the obtained Ce encapsulated Beta zeolites exhibit superior activity and stability in the liquid alkylation between benzene and 1-dodecene, because the additional Ce species not only increase the concentration of local olefins neighboring Brønsted acid sites through the adsorption of olefins, promoting the generation of dodecyl carbenium ions, but also inhibit the self-polymerization of 1-dodecene on a certain degree through activating the benzene molecules. Furthermore, the resultant Ce encapsulated Beta zeolites also exhibit robust regeneration ability, which is crucial for their application in the practical alkylation reaction of aromatics.

Declaration of Interest

The authors declare that they have no known competing financial interests or personal relationships that could have appeared to influence the work reported in this paper.

Acknowledgements

This work was supported by the National Natural Science Foundation of China (22278090, 21978055), Natural Science Foundation of Guangdong Province, China (2022A1515012088), the Science and Technology Planning Project of Guangdong Province, China (2022A0505030073, 2022A0505030013).

Supplementary Material

Supplementary data to this article can be found online at https://doi.org/10.1016/j.cjche.2023.11.007.

Experimental content of preparation and characterization of Beta zeolite; particle size distribution and acidity data of resultant Beta zeolites; XPS data of Beta-3Ce; ^{1}H MAS NMR spectra of Beta-0Ce and Beta-3Ce; conversion of 1-dodecene and 2-LAB selectivity of Beta-3Ce at different WHSV; TG curve and productivity of coke of spent Beta zeolites; XRD patterns, N_2 adsorption–desorption isotherms, textural parameters of fresh, regeneration and spent Beta-3Ce; SEM images, particle size distribution, FTIR spectra of pyridine and 2, 6-di-*tert*-butylpyridine adsorption and acidity data of Beta-3Ce and Beta-3Ce-R; TG curve of spent Beta-3Ce and spent Beta-3Ce-R are included.

References

[1] R.M. Li, S.Y. Xing, S.A. Zhang, M.H. Han, Effect of surface silicon modification of H-beta zeolites for alkylation of benzene with 1-dodecene, *RSC Adv.* 10 (17) (2020) 10006–10016.
[2] J.J. Wang, Y.Y. Chuang, H.Y. Hsu, T.C. Tsai, Toward industrial catalysis of zeolite for linear alkylbenzene synthesis: A mini review, *Catal. Today* 298 (2017) 109–116.
[3] A. Aitani, J.B. Wang, I. Wang, S. Al-Khattaf, T.C. Tsai, Environmental benign catalysis for linear alkylbenzene synthesis: A review, *Catal. Surv. Asia* 18 (1) (2014) 1–12.

[4] G. Zahedi, H. Yaqubi, M. Ba-Shammakh, Dynamic modeling and simulation of heavy paraffin dehydrogenation reactor for selective olefin production in linear alkyl benzene production plant, *Appl. Catal. A* 358 (1) (2009) 1–6.

[5] M.H. Han, Z. Cui, C. Xu, W. Chen, Y. Jin, Synthesis of linear alkylbenzene catalyzed by Hβ-zeolite, *Appl. Catal. A* 238 (1) (2003) 99–107.

[6] T.C. Tsai, I. Wang, S.J. Li, J.Y. Liu, Development of a green LAB process: Alkylation of benzene with 1-dodecene over mordenite, *Green Chem.* 5 (4) (2003) 404–409.

[7] J.G. Ma, B.J. Boyd, C.J. Drummond, Positional isomers of linear sodium dodecyl benzene sulfonate: Solubility, self-assembly, and air/water interfacial activity, *Langmuir* 22 (21) (2006) 8646–8654.

[8] J.L.G. de Almeida, M. Dufaux, Y. Ben Taarit, C. Naccache, Linear alkylbenzene, *J. Am. Oil Chem. Soc.* 71 (7) (1994) 675–694.

[9] J.A. Kocal, B.V. Vora, T. Imai, Production of linear alkylbenzenes, *Appl. Catal. A* 221 (1–2) (2001) 295–301.

[10] S. Sivasanker, A. Thangaraj, Distribution of isomers in the alkylation of benzene with long-chain olefins over solid acid catalysts, *J. Catal.* 138 (1) (1992) 386–390.

[11] C. Perego, P. Ingallina, Recent advances in the industrial alkylation of aromatics: New catalysts and new processes, *Catal. Today* 73 (1–2) (2002) 3–22.

[12] C. DeCastro, E. Sauvage, M.H. Valkenberg, W.F. Hölderich, Immobilised ionic liquids as lewis acid catalysts for the alkylation of aromatic compounds with dodecene, *J. Catal.* 196 (1) (2000) 86–94.

[13] G.P. Qi, F. Jiang, X.W. Sun, S.Q. Zhao, Alkylation mechanism of benzene with 1-dodecene catalyzed by Et_3NHCl-$AlCl_3$, *Sci. China Chem.* 53 (5) (2010) 1102–1107.

[14] H.L. Xin, Q. Wu, M.H. Han, D.Z. Wang, Y. Jin, Alkylation of benzene with 1-dodecene in ionic liquids $[Rmim]^+Al_2Cl_6X^-$ (R = butyl, octyl and dodecyl; X = chlorine, bromine and iodine), *Appl. Catal. A* 292 (2005) 354–361.

[15] H.O. Zhu, X.Q. Ren, J. Wang, A comparative study of the catalytic behavior of SBA-15 supported heteropoly acid $H_3PW_{12}O_{40}$ and H-Y catalysts in the alkylation of benzene with 1-dodecene, *React. Kinet. Catal. Lett.* 83 (1) (2004) 19–24.

[16] J.C. Zhang, B.H. Chen, C.Y. Li, Z.G. Zhu, L.Y. Wen, E.Z. Min, Kinetics of benzene alkylation with 1-dodecene over a supported tungstophosphoric acid catalyst, *Appl. Catal. A* 249 (1) (2003) 27–34.

[17] J.C. Zhang, Z.G. Zhu, C.Y. Li, L.Y. Wen, E.Z. Min, Characterization and kinetic investigation of tungstophosphoric supported on SiO_2 for alkylation of benzene with 1-dodecene to synthesize linear alkylbenzene, *J. Mol. Catal.* 198 (1–2) (2003) 359–367.

[18] M.A. Harmer, Q. Sun, Solid acid catalysis using ion-exchange resins, *Appl. Catal. A* 221 (1–2) (2001) 45–62.

[19] J.H. Clark, G.L. Monks, D.J. Nightingale, P.M. Price, J.F. White, A new solid acid-based route to linear alkylbenzenes, *J. Catal.* 193 (2) (2000) 348–350.

[20] F. Zarkesh, F. Farzaneh, A.M. Ghandi, Metal ions exchanged montmorillonite as catalyst for alkylation of benzene with 1-dodecene, *React. Kinet. Catal. Lett.* 89 (2) (2006) 247–252.

[21] B.Y. Liu, Z.T. Liao, Y. Wu, C.H. Ding, F.S. Butt, Y. Huang, J.X. Dong, Efficient production of linear alkylbenzene by liquid alkylation between benzene and 1-dodecene over MWW zeolites, *Mol. Catal.* 531 (2022) 112642.

[22] X.D. Yuan, J.N. Park, J. Wang, C.W. Lee, S.E. Park, Alkylation of benzene with 1-dodecene over usy zeolite catalyst: Effect of pretreatment and reaction conditions, *Korean J. Chem. Eng.* 19 (4) (2002) 607–610.

[23] W. Aslam, M.A.B. Siddiqui, B. Rabindran Jermy, A. Aitani, J. Čejka, S. Al-Khattaf, Selective synthesis of linear alkylbenzene by alkylation of benzene with 1-dodecene over desilicated zeolites, *Catal. Today* 227 (2014) 187–197.

[24] S.Y. Xing, T.F. Wang, M.H. Han, Effect of different frameworks on the zeolite catalyzed alkylation of benzene with 1-dodecene, *Mol. Catal.* 531 (2022) 112644.

[25] J.S. Lin, J.J. Wang, J. Wang, I. Wang, R.J. Balasamy, A. Aitani, S. Al-Khattaf, T.C. Tsai, Catalysis of alkaline-modified mordenite for benzene alkylation of diolefin-containing dodecene for linear alkylbenzene synthesis, *J. Catal.* 300 (2013) 81–90.

[26] M. Horňáček, P. Hudec, A. Smiešková, T. Jakubík, Alkylation of benzene with 1-alkenes over beta zeolite in liquid phase, *React. Kinet. Mech. Catal.* 99 (2) (2010) 431–437.

[27] M. Horňáček, P. Hudec, A. Nociar, A. Smiešková, T. Jakubík, Activity and regenerability of dealuminated zeolite Y in liquid phase alkylation of benzene with 1-alkene, *Chem. Pap.* 64 (4) (2010) 469–474.

[28] Y. Cao, Alkylation of benzene with dodecene. The activity and selectivity of zeolite type catalysts as a function of the porous structure, *Appl. Catal. A* 184 (2) (1999) 231–238.

[29] B. Thomas, S. Sugunan, Alkylation of benzene with 1-octene over rare earth exchanged HFAU-Y zeolites, *React. Kinet. Catal. Lett.* 85 (1) (2005) 29–36.

[30] Z.K. Zhao, W.H. Qiao, G.R. Wang, Z.S. Li, L. Cheng, Alkylation of α-methylnaphthalene with long-chain olefins catalyzed by rare earth lanthanum modified HY zeolite, *J. Mol. Catal.* 250 (1–2) (2006) 50–56.

[31] N. Wang, Q.M. Sun, R.S. Bai, X. Li, G.Q. Guo, J.H. Yu, *In situ* confinement of ultrasmall Pd clusters within nanosized silicalite-1 zeolite for highly efficient catalysis of hydrogen generation, *J. Am. Chem. Soc.* 138 (24) (2016) 7484–7487.

[32] Q.M. Sun, N. Wang, Q.M. Bing, R. Si, J.Y. Liu, R.S. Bai, P. Zhang, M.J. Jia, J.H. Yu, Subnanometric hybrid Pd-$M(OH)_2$, M = Ni, Co, clusters in zeolites as highly efficient nanocatalysts for hydrogen generation, *Chem* 3 (3) (2017) 477–493.

[33] H. Wang, L.A. Wang, F.S. Xiao, Metal@zeolite hybrid materials for catalysis, *ACS Cent. Sci.* 6 (10) (2020) 1685–1697.

[34] W.L. Han, Z.C. Tang, P. Zhang, G.X. Lu, Study of one step synthesis of rare earth zeolite (In-ZSM-5) and application for low temperature CO catalytic oxidation, *Catal. Surv. Asia* 17 (3) (2013) 147–155.

[35] E. Bèche, P. Charvin, D. Perarnau, S. Abanades, G. Flamant, Ce 3d XPS investigation of cerium oxides and mixed cerium oxide ($Ce_xTi_yO_z$), *Surf. Interface Anal.* 40 (2008) 264–267, 2008.

[36] Z.J. Wu, S. Goel, M. Choi, E. Iglesia, Hydrothermal synthesis of LTA-encapsulated metal clusters and consequences for catalyst stability, reactivity, and selectivity, *J. Catal.* 311 (2014) 458–468.

[37] W.M. Hao, W.M. Zhang, Z.B. Guo, J.H. Ma, R.F. Li, Mesoporous beta zeolite catalysts for benzylation of naphthalene: Effect of pore structure and acidity, *Catalysts* 8 (11) (2018) 504.

[38] J. Fahy, D.L. Trimm, D.J. Cookson, Four component catalysis for the hydroalkylation of benzene to cyclohexyl benzene, *Appl. Catal. A* 211 (2) (2001) 259–268.

[39] S. Inagaki, K. Kamino, E. Kikuchi, M. Matsukata, Shape selectivity of MWW-type aluminosilicate zeolites in the alkylation of toluene with methanol, *Appl. Catal. A* 318 (2007) 22–27.

[40] J. Pérez-Ramírez, J.C. Groen, A. Brückner, M.S. Kumar, U. Bentrup, M.N. Debbagh, L.A. Villaescusa, Evolution of isomorphously substituted iron zeolites during activation: Comparison of Fe-beta and Fe-ZSM-5, *J. Catal.* 232 (2) (2005) 318–334.

[41] R.A. García-Muñoz, D.P. Serrano, G. Vicente, M. Linares, D. Vitvarova, J. Čejka, Remarkable catalytic properties of hierarchical zeolite-Beta in epoxide rearrangement reactions, *Catal. Today* 243 (2015) 141–152.

[42] X.F. Zhang, R.J. Wang, X.X. Yang, Effect of alkaline treatment on pore structure and acidity of HZSM-5 in the synthesis of ethyl mercaptan, *Catal. Commun.* 60 (2015) 32–36.

[43] K. Góra-Marek, K. Tarach, M. Choi, 2, 6-di-*tert*-butylpyridine sorption approach to quantify the external acidity in hierarchical zeolites, *J. Phys. Chem. C* 118 (23) (2014) 12266–12274.

[44] J.J. Huang, B.Y. Liu, Z.T. Liao, H.Y. Chen, K. Yan, Fabrication of Cu-encapsulated hierarchical MEL zeolites for alkylation of mesitylene with benzyl alcohol, *Ind. Eng. Chem. Res.* 58 (36) (2019) 16636–16644.

[45] V. Pashkova, P. Klein, J. Dedecek, V. Tokarová, B. Wichterlová, Incorporation of Al at ZSM-5 hydrothermal synthesis. Tuning of Al pairs in the framework, *Microporous Mesoporous Mater.* 202 (2015) 138–146.

[46] J. Dedecek, V. Balgová, V. Pashkova, P. Klein, B. Wichterlová, Synthesis of ZSM-5 zeolites with defined distribution of Al atoms in the framework and multinuclear MAS NMR analysis of the control of Al distribution, *Chem. Mater.* 24 (16) (2012) 3231–3239.

[47] Y.Y. Ji, C.Y. Wang, Y.C. Zou, J.W. Song, J.Y. Wang, F. Li, F.S. Xiao, Design and synthesis of microporous and micro/mesoporous silica materials with excellent adsorption properties *via* self-assembly of silica species with tetraethyl ammonium in acidic aqueous media, *J. Phys. Chem. C* 112 (49) (2008) 19367–19371.

[48] M. Hunger, Brønsted acid sites in zeolites characterized by multinuclear solid-state NMR spectroscopy, *Catal. Rev.* 39 (4) (1997) 345–393.

[49] R.R. Pinto, P. Borges, M.A.N.D.A. Lemos, F. Lemos, J.C. Védrine, E.G. Derouane, F.R. Ribeiro, Correlating NH_3-TPD and ^1H MAS NMR measurements of zeolite acidity: Proposal of an acidity scale, *Appl. Catal. A* 284 (1–2) (2005) 39–46.

[50] Z.M. Yan, D. Ma, J.Q. Zhuang, X.C. Liu, X.M. Liu, X.W. Han, X.H. Bao, F.X. Chang, L. Xu, Z.M. Liu, On the acid-dealumination of USY zeolite: A solid state NMR investigation, *J. Mol. Catal.* 194 (1–2) (2003) 153–167.

[51] M. Müller, G. Harvey, R. Prins, Comparison of the dealumination of zeolites beta, mordenite, ZSM-5 and ferrierite by thermal treatment, leaching with oxalic acid and treatment with $SiCl_4$ by ^1H, ^{29}Si and ^{27}Al MAS NMR, *Microporous Mesoporous Mater.* 34 (2) (2000) 135–147.

[52] E.G. Derouane, J.C. Védrine, R.R. Pinto, P.M. Borges, L. Costa, M.A.N.D.A. Lemos, F. Lemos, F.R. Ribeiro, The acidity of zeolites: Concepts, measurements and relation to catalysis: A review on experimental and theoretical methods for the study of zeolite acidity, *Catal. Rev.* 55 (4) (2013) 454–515.

[53] I. Fechete, A. Simon-Masseron, E. Dumitriu, D. Lutic, P. Caullet, H. Kessler, The role of acidity of CeH–EMT–type zeolite for catalyzing toluene alkylation with methanol to xylenes, *Rev. Roum. Chim.* 53 (2008) 55–61.

[54] L.H. Duan, Z.L. Sun, D.S. Liu, Z.H. Dai, X.Q. Li, L.J. Song, Adsorption and diffusion of thiophene, benzene, *n*-octane, and 1-octene on FAU zeolites, *Stud. Surf. Sci. Catal.* 170 (2007) 910–917.

[55] L.H. Duan, X.H. Gao, X.H. Meng, H.T. Zhang, Q.A. Wang, Y.C. Qin, X.T. Zhang, L.J. Song, Adsorption, co-adsorption, and reactions of sulfur compounds, aromatics, olefins over Ce-exchanged Y zeolite, *J. Phys. Chem. C* 116 (49) (2012) 25748–25756.

[56] H.G. Wang, L.J. Song, H. Jiang, J. Xu, L.L. Jin, X.T. Zhang, Z.L. Sun, Effects of olefin on adsorptive desulfurization of gasoline over Ce(IV)Y zeolites, *Fuel Process. Technol.* 90 (6) (2009) 835–838.

[57] I. Craciun, M.F. Reyniers, G.B. Marin, Liquid-phase alkylation of benzene with octenes over Y zeolites: Kinetic modeling including acidity descriptors, *J. Catal.* 294 (2012) 136–150.

[58] V.R. Choudhary, S.K. Jana, Benzylation of benzene and substituted benzenes by benzyl chloride over $InCl_3$, $GaCl_3$, $FeCl_3$ and $ZnCl_2$ supported on clays and Si-MCM-41, *J. Mol. Catal.* 180 (1–2) (2002) 267–276.